Inorganics **2014**, 2, 248-263; doi:10.3390/inorganics2020248

OPEN ACCESS

inorganics

ISSN 2304-6740

www.mdpi.com/journal/inorganics

Article

From Stable ZnO and GaN Clusters to Novel Double Bubbles and Frameworks

Matthew R. Farrow [1], John Buckeridge [1], C. Richard A. Catlow [1], Andrew J. Logsdail [1], David O. Scanlon [1,2], Alexey A. Sokol [1] and Scott M. Woodley [1,*]

[1] Department of Chemistry, Kathleen Lonsdale Materials Chemistry, University College London, 20 Gordon Street, London WC1H 0AJ, UK; E-Mails: m.farrow@ucl.ac.uk (M.R.F.); j.buckeridge@ucl.ac.uk (J.B.); c.r.a.catlow@ucl.ac.uk (C.R.A.C.); a.logsdail@ucl.ac.uk (A.J.L.); d.scanlon@ucl.ac.uk (D.O.S.); a.sokol@ucl.ac.uk (A.A.S.)

[2] Diamond Light Source Ltd., Diamond House, Harwell Science and Innovation Campus, Didcot, Oxfordshire OX11 0DE, UK

***** Author to whom correspondence should be addressed; E-Mail: scott.woodley@ucl.ac.uk; Tel.: +44-20-7679-0315; Fax: +44-20-7679-0493.

Received: 1 April 2014; in revised form: 4 May 2014 / Accepted: 5 May 2014 / Published: 28 May 2014

Abstract: A bottom up approach is employed in the design of novel materials: first, gas-phase "double bubble" clusters are constructed from high symmetry, T_h, 24 and 96 atom, single bubbles of ZnO and GaN. These are used to construct bulk frameworks. Upon geometry optimization—minimisation of energies and forces computed using density functional theory—the symmetry of the double bubble clusters is reduced to either C_1 or C_2, and the average bond lengths for the outer bubbles are 1.9 Å, whereas the average bonds for the inner bubble are larger for ZnO than for GaN; 2.0 Å and 1.9 Å, respectively. A careful analysis of the bond distributions reveals that the inter-bubble bonds are bi-modal, and that there is a greater distortion for ZnO. Similar bond distributions are found for the corresponding frameworks. The distortion of the ZnO double bubble is found to be related to the increased flexibility of the outer bubble when composed of ZnO rather than GaN, which is reflected in their bulk moduli. The energetics suggest that $(ZnO)_{12}@(GaN)_{48}$ is more stable both in gas phase and bulk frameworks than $(ZnO)_{12}@(ZnO)_{48}$ and $(GaN)_{12}@(GaN)_{48}$. Formation enthalpies are similar to those found for carbon fullerenes.

Keywords: double bubbles; zinc oxide; gallium nitride; density functional theory

1. Introduction

A new class of materials is sought that will support the separation of electrons and holes typically generated during photo-excitation by solar radiation. In this context, heterostructures of ZnO/GaN attract particular interest, as such materials have great potential in a wide range of applications from semiconductor optoelectronics to photo-catalysis [1–5].

Previous computational simulations [6–8] have predicted that both ZnO and GaN, at the nanoscale, form clusters with a bubble architecture that are dramatically different from models cut from their wurtzite bulk structures. Using ZnO and SiC as two simple examples, we have shown [9,10] how individual bubbles can combine to form extended framework materials; alternative constructions and the viability (or stability) of similar frameworks using bubbles as building blocks have also been reported [6,9–11]. For framework structures, an increase in density is typically correlated with an enhanced stability, which can be achieved by connecting appropriate building units. In our approach to framework construction, we choose a new type of unit, the so-called "double bubble", that are themselves denser than single-shell bubbles and which are a preferred motif for larger sized clusters [12].

For binary oxide and semiconductor II-VI and III-V materials with a 1-1 stoichiometry, fullerene type structures have been the focus of materials modelling at the nanoscale in the last decade. This interest has partly been spurred by reports of synthesis of $(MX)_n$ clusters of these materials, where M denotes metals, or cations, and X represents anions, with the mass spectra of such systems showing unexpected preference for certain sizes *n*. The preferred values of *n* are widely known as "magic numbers" [8]. The stability of such clusters has been explained on thermodynamic grounds: the binding energy per formula unit as a function of size having a minimum (*i.e.*, the energy released on cluster formation has a maximum). Alternative explanations have been proposed using: (i) a kinetic argument based on whether the cluster growth or shrinkage is an energetically favourable process; and (ii) a statistical argument: a particular cluster size may be realized in a greater number of atomic configurations compared to others, and therefore is favoured entropically. For any particular experiment, one or a combination of these factors may in fact be relevant.

Considering the atomic structure of stable clusters as a function of increasing size, we recognise an evolution of basic structural units with increasing dimensionality: from 1D—sticks; to 2D—rings and patchworks of rings; and then to 3D units that are initially composed of one layer—a tube or bubble—and then multiple layers, and finally bulk like phases (those that could be stable or metastable on the macroscopic scale). The bubble structures are also denoted in the literature as cages, spheroids, or fullerenes. The above classification is also based on the atomic connectivity or bonding, which increases with increased dimensionality. Using additional definitions given in reference [13], perfect closed bubbles are an important subclass of single walled fullerene-like clusters, in which each atom has three nearest neighbours, and the surface of such fullerenes is composed of a patchwork of hexagonal faces that is wrapped in three dimensions by the introduction of six "defects", or tetragonal faces. The existence and stability of the fullerene-like inorganic structures have been known from both theory and experiment for BN, ZnO, and MoS_2 [14–16]. Perfect bubbles can also include larger

patches with an even number of sides complemented by an appropriate number of tetragonal faces. In contrast to carbon fullerenes, pentagonal faces are not realised for the heterogeneous semiconductor class of compound, as they would require formation of M–M and/or X–X bonds that are electrostatically unfavourable. Due to the ionic nature of bonding in these materials, the charge disproportionation is not compatible with electron localisation, required for metal-metal bond formation, or hole localisation, which stabilises di-oxygen or di-nitrogen species.

On further size increase (cluster growth), the appearance of layered structures becomes a possibility, in which a smaller sized cluster unit is contained within a larger bubble structure. Indeed, such structures have been discovered in molecular dynamical studies of ZnS, where the smallest is found for n = 60: an n = 48 bubble forms a concentric shell around an n = 12 sodalite cage [12]. Although both single bubbles have the same high symmetry T_h point group, the double bubble can relax into a lower symmetry form depending on the composition. The T_h symmetry unit, however, can be stabilised when this unit is used in frameworks that were constructed previously from the individual single layered components.

In this paper, we investigate the different possible atomic structural relaxations of the double bubble and the effect of mixing components of different compositions, for both the individual clusters and the constructed frameworks.

2. Construction of Double Bubbles

High Symmetry Double Bubble Clusters as Secondary Building Units

We consider the 1-1 compounds that are predicted to have stable (lowest energy for a particular size) and metastable bubble, or fullerene like, structures. Perfect versions of these structures are composed of only three-coordinated atoms, sets of which create rings with an even number of sides that can be visualised as one of the faces of the bubble; an odd number of sides is unlikely as this would require at least one neighbouring pair of vertices of only cations or anions. Except for the smallest sized clusters, in which the curvature of the layer is important, cluster configurations containing one- or two-coordinated atoms are less stable than the perfect bubbles. Another characteristic of the stable bubbles is that, typically, the number of tetragonal rings is minimised (and, to a lesser extent, the distance between these should be maximised), while the number of hexagonal rings is maximised. A layer consisting of only hexagonal rings has no curvature, and therefore a perfect bubble of hexagons would require an infinite number of atoms (*i.e.*, a 2D infinite hexagonal sheet). To obtain a perfect bubble with a finite number of atoms, the sheet requires the introduction of six tetragonal rings (Euler's rule) as each tetragonal ring increases the curvature of the sheet. Increasing the number of tetragonal rings results in open (as opposed to closed) perfect bubbles, which contain much larger rings, e.g., octagonal, assuming the chemistry of the compound does not favour the bonding and coordination required for the formation of cuboids, *i.e.*, cuts from rock salt.

The higher symmetry configurations of the perfect bubbles are typically found to be more stable. As high symmetry cluster structures are only possible for certain sizes, they are not only the stable state for their particular size, but usually have a greater stability than clusters of neighbouring sizes. In our previous studies [6,9,10] we have, therefore, focused our attention on families of high symmetry

structures, and, in particular, those with symmetry T_h, T_d and T. These $(MX)_n$ structures are found if n = 4 (T_d), 12 (T_h), 16 (T_d), 28 (T), 36 (T_d), 48 (T_h), 64 (T_d), … Larger T_h and T_d clusters include n = 108 and 192 and n =100, 144 and 196, respectively; examples are shown in Figure 1. These clusters can be visualised as truncated octahedra, where there is one tetragonal ring of the bubble at each of the six truncated corners, and the hexagonal patchworks form the octahedron's faces. In this morphology, the distance between all tetragonal rings is maximised for a given size n, and the separation increases monotonically with n.

Figure 1. Models of high symmetry $(MX)_n$ bubbles with: (**a**) n = 12 with symmetry T_h; (**b**) n = 48 with symmetry T_h; (**c**) n = 28, 36 and 48 with octahedra superimposed.

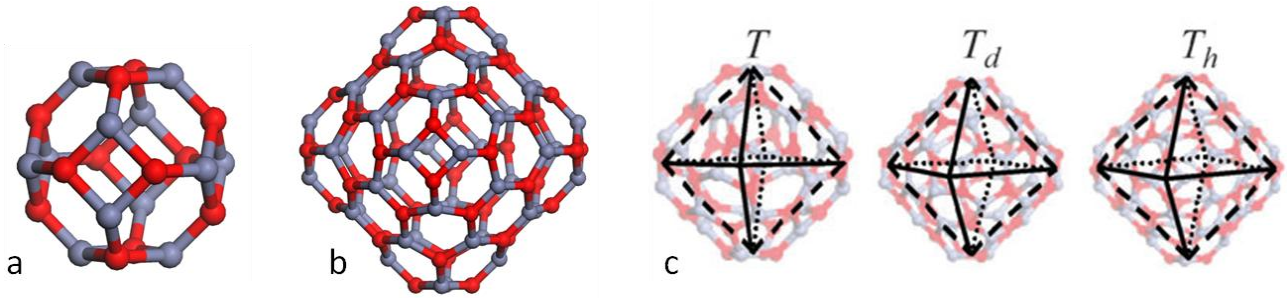

Smaller bubble clusters can be readily generated using an appropriate global optimiser (e.g., one based on Monte Carlo basin hopping [17] or genetic algorithm [18] routines), and once one has determined the relationship between them, the larger bubble clusters can be constructed by simply increasing the number of rows of hexagonal rings in each face or edge of the octahedron. For example, each octahedron's edge of a T_d bubble links a side of two tetragonal rings via a "ladder" of m hexagonal rings (one hexagon wide)—see the highlighted ladder in Figure 2a—with the remaining hexagonal rings completing the faces of the octahedron. Note that the line of the octahedron edge bisects the rings of this ladder and that the tetragonal ring is out of phase with the tetragonal face created by truncating the octahedron. Constructions with m = 0, 1, 2, 3, 4 and 5 corresponds to perfect bubbles at n = 4, 16, 36, 64, 100, 144 and 196, respectively. In contrast, each octahedron edge in a T_h bubble links the corner of two tetragonal rings via m + 1 M–X sticks that are separated by m hexagonal rings, forming an alternating linear pattern. Each stick is actually a shared side of two hexagonal rings, with each ring part of a hexagonal patchwork that covers a face of the octahedron. These sticks form a line segment of the octahedron edge (see highlighting in Figure 2b), and this line bisects opposite angles of the hexagonal rings, rather than opposite sides, and the tetragonal rings are in-phase with the tetragonal face created by truncating the octahedron. The smallest T_h bubble, m = 0, or n = 12, has just one stick between two neighbouring tetragonal rings. The next smallest size T_h bubble, m = 1, or n = 48, is constructed using two sticks and one hexagonal ring; then, for m = 2, or n = 108, there are three sticks and two hexagonal rings. Comparing the growth of the octahedron edges, it is evident why there are more bubbles with T_d rather than T_h symmetry.

Figure 2. Models of high symmetry $(MX)_n$ bubbles with: (**a**) n = 64, symmetry T_d and the ladder of hexagonal rings, highlighted in yellow, that corresponds to one of the twelve edges of an octahedron; (**b**) n = 48, symmetry T_h with a fragment that corresponds to one of twelve edges highlighted in yellow; (**c**) n = 48, symmetry T_h with one of twelve patchworks that correspond to the octahedron side highlighted in purple.

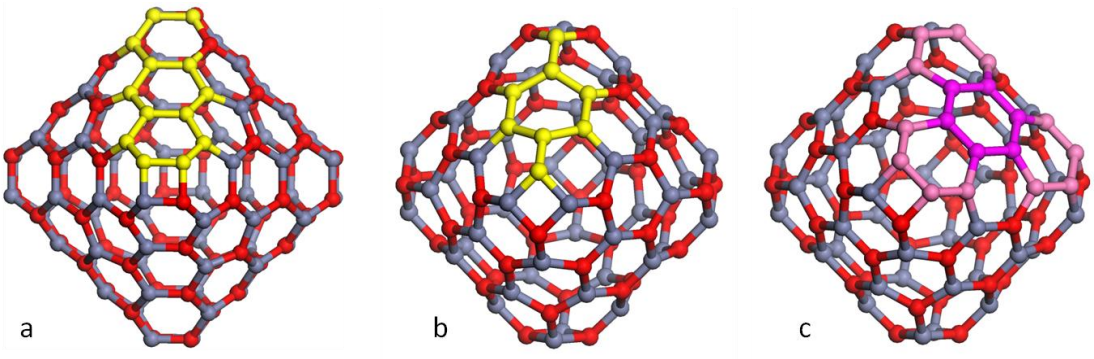

As discussed in the Introduction, framework structures with an increased density are typically more stable [19,20]. We therefore choose to investigate double bubbles that are composed of high symmetry perfect bubbles as these are more dense. Two bubbles are combined by inserting the smaller bubble inside the larger; aligned with the same centre of mass and identical direction of orthogonal axes, with each axis passing through the centre of mass and the centre of opposite truncated corners, or tetragonal faces. The rotation of these tetragonal faces about the octahedral axes is dependent upon the symmetry of the cluster. When clusters have T_h and T_d symmetry this rotation is 45 ° out-of-phase, and, if one of the bubbles has T symmetry, between 0 ° and 45 °. For stability, the best match is obtained when the inner and outer bubbles are taken from the set of T_h bubbles and the highest density obtained by combining the smallest two of these: n = 12 (a sodalite cage) and n = 48 [10].

In the MX bulk phase considered here, the atoms are four-coordinated tetrahedra, so the stability of the double bubbles will improve if M–X linkages between layers are found. These linkages can be expected to be located between aligned pairs of hexagonal patchworks that form the faces of the octahedra rather than between the truncated corners. For the n = 60 double bubble, the inner n = 12 bubble has one hexagonal ring on each face, whereas the outer n = 48 bubble is composed of a patchwork of five and a half hexagonal rings; a central hexagonal ring that is linked via one hexagonal ring to each of three nearest tetragonal rings and three hexagonal rings that are shared with neighbouring faces of the octahedron (see Figure 2c). Importantly, the central hexagonal ring can bond with the hexagonal ring of the inner bubble; see Figure 3. Analogous to our structures, experimentally observed cages of boron nitride (BN), [15,16] and molybdenum sulphide (MoS_2) [21,22] have been reported to be constructed from four and six (hexagonal) membered ring building units. CdSe cage structures have been experimentally observed to be stable and formed from truncated-octahedra [23]. DFT calculations on cage structures of CdSe that are similar to our structures have also been reported [24].

Figure 3. Models of the $n = 60$ T_h double bubble, with inter-layer links between the inner $n = 12$ sodalite cage and the eight hexagonal rings that are in the centres of the octahedron faces of the outer $n = 48$ bubble, highlighted using ball-and-sticks rather than line representation for: (**a**) no bridging links; (**b**) four bridging links; and (**c**) all eight bridging links.

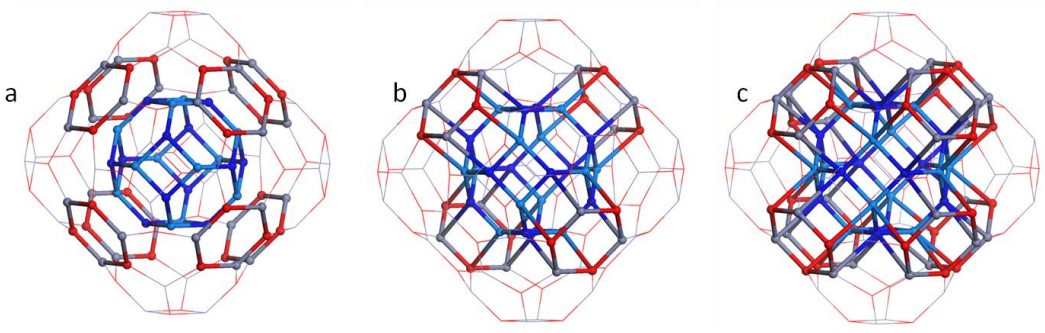

The first framework is constructed from T_h bubble (sodalite cage) secondary building units (SBUs) of $(ZnO)_{12}$ and $(GaN)_{12}$, see Figure 1a. As the typical Zn–O and Ga–N bond lengths are similar (1.98 Å and 1.95 Å in their ground state wurtzite form), their respective SBUs are also similar in size. Consider each SBU as an octahedron. By corner sharing the octahedra, and assuming an equal number of SBUs for each compound, we construct an fcc, rock-salt like lattice, as shown in Figure 4c. The second framework is constructed from the $n = 60$ T_h double bubbles; see Figures 1c and 4b. Again, imagining each SBU as an octahedron, but rather than corner sharing they are now stacked so that they share edges, each double bubble is surrounded by twelve others (see Figure 4d), and each edge of the outer bubble is one bond length from an edge of a neighbouring bubble forming an $n = 6$ double ring (a drum) and two $n = 2$ rings. Each tetragonal ring of an outer $n = 48$ bubble combines with five others to form an $n = 12$ T_h bubble, *i.e.*, the void is a sodalite cage. The inner sodalite cage of each double bubble is formed from (i) the same compound and (ii) two compounds, which we alternate.

We start the double bubble construction from two relaxed single bubbles. If the distance between each inner hexagonal ring and its corresponding central hexagonal ring of the outer bubble is approximately a typical M–X bond length, then we shall refer to this as an ideal match, and the relaxed double bubble is expected to maintain T_h symmetry. Whether there is an ideal match depends on the composition: if the two layers are of the same composition and there is not an ideal match then the inner bubble is too small. The outer eight planes of hexagonal patchworks, or octahedron faces, have more flexibility than the corners. During a geometry relaxation of the double bubble, the central hexagonal ring of each outer patchwork can move inward, maintaining the T_h symmetry or, due to the repulsion between neighbouring patchworks, only the central hexagons from alternate patchworks, *i.e.*, four of the eight, move inwards reducing the symmetry to T; see Figure 3.

For all ZnO/GaN compositions investigated here, $n = 60$ double bubble structures of high symmetry (T_h and T) were constructed and then geometry optimised. Low symmetry structural distortions were allowed in the optimisation process in order to find the lowest energy double bubble configuration.

Figure 4. Ball and stick models of two framework structures. (**a**) Constructed from T_h bubbles of $(GaN)_{12}$ and $(ZnO)_{12}$; (**b**) Constructed from T_h double bubbles of $(ZnO)_{48}$ and $(GaN)_{12}$; (**c**) the same structure as (a) but with each $(GaN)_{12}$ coloured red and each $(ZnO)_{12}$ coloured blue (lighter/darker shades used in the front/back row); (**d**) the same structure as (b) but with each $(GaN)_{12}$ hidden and each $(ZnO)_{48}$ uniquely coloured.

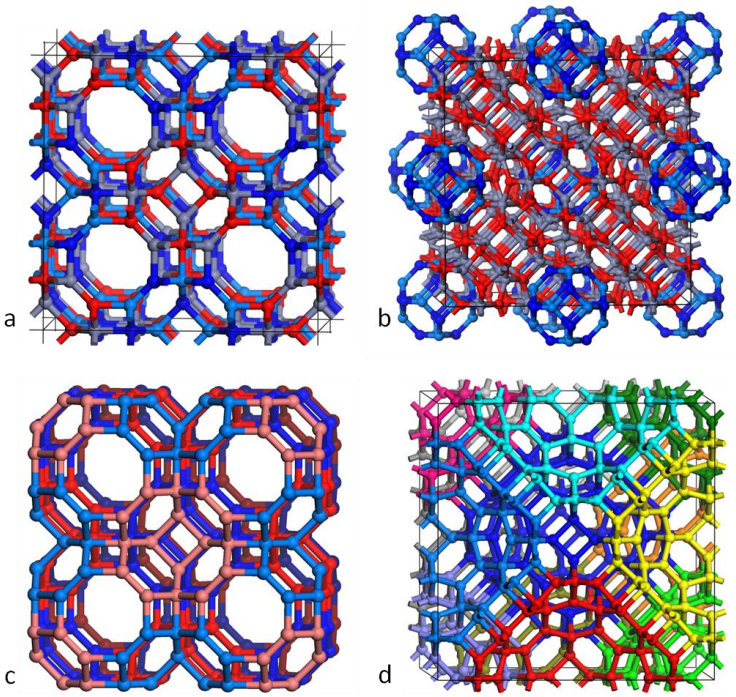

3. Results and Discussion

3.1. Double Bubble Clusters

With each layer (single bubble) composed of either ZnO or GaN, there are four possible $n = 60$ double bubble structures that can be constructed using the procedure discussed in Section 2. The cluster structures are relaxed so as to minimise the energy, which is initially defined using a semi-empirical potentials and then, during a final refinement stage, using density functional theory (DFT); see Sections 4.1 and 4.2 for details. The four double bubble clusters consist of: (a) only zinc oxide, denoted $(ZnO)_{12}@(ZnO)_{48}$; (b) only gallium nitride, denoted $(GaN)_{12}@(GaN)_{48}$; (c) a gallium nitride sodalite cage inside a zinc oxide bubble, denoted $(GaN)_{12}@(ZnO)_{48}$; and the inverse (d) a zinc oxide sodalite cage inside a gallium nitride bubble, denoted $(ZnO)_{12}@(GaN)_{48}$. During geometry optimization, although the high T_h and T symmetry that is maintained when semi-empirical calculations are employed, there is a reduction of symmetry for all four systems to C_n, where $n = 1$ or 2. As reported in Table 1, double bubble clusters with internal $(ZnO)_{12}$ sodalite cages adopt C_2 symmetry, whereas those that had gallium nitride sodalite cages adopt C_1 symmetry—*i.e.*, there is no symmetry in those structures. The average relaxed bond lengths, separated into inner-bubble bonds, outer-bubble bonds, and inter-layer bubble bonds (M–X bonds connecting the inner to the outer bubbles) are also reported in Table 1. The average bond lengths of zinc oxide and gallium nitride are

similar; although the average bond length for zinc oxide inner bubbles are slightly greater than the average bond lengths of gallium nitride inner bubbles.

Now, consider the distribution of bond lengths, $G(x)$, using a Gaussian broadening function for each bond length, which is normalised to the number of linkages between the inner and outer bubble (N = 48 for our n = 60 double bubbles):

$$G(x) = C\sum_{i=1}^{N} \exp(b_i - x)^2/2\sigma^2 \quad (1)$$

C is a normalising constant, b_i is the length of bond i, and σ is the dispersion (width) of the Gaussian function. This function is plotted in Figure 5 for two values of σ: 0.02 Å (red line) and 0.10 Å (blue line). The greater value of σ allows the resolution of two distinct peaks for the systems of interest. These two peaks are reported in Table 1, labelled as *A* and *B* inter-bubble bond distances.

Table 1. Structural parameters of double bubble clusters, where D_{outer} is the mean distance between M–X atoms in the outer bubble, D_{inner} is the mean distance between M–X atoms in the inner bubble, and D_{inter} is the distance between the inner and outer bubbles. (Number in parentheses indicates standard error.)

System	Symmetry	D_{outer} (Å)	D_{inner} (Å)	D_{inter} (Å)	
				A	***B***
$(GaN)_{12}@(ZnO)_{48}$	C1	1.92	1.93	2.05 (0.1)	3.08 (0.1)
$(ZnO)_{12}@(GaN)_{48}$	C2	1.89	1.96	2.13 (0.1)	2.94 (0.1)
$(ZnO)_{12}@(ZnO)_{48}$	C2	1.93	1.95	2.10 (0.0)	2.94 (0.2)
$(GaN)_{12}@(GaN)_{48}$	C1	1.93	1.92	2.10 (0.1)	2.94 (0.1)

Figure 5. Bond distribution plots for the double bubble cluster systems. Red line: Dispersion of Gaussian = 0.02, Blue line: Dispersion of Gaussian = 0.1.

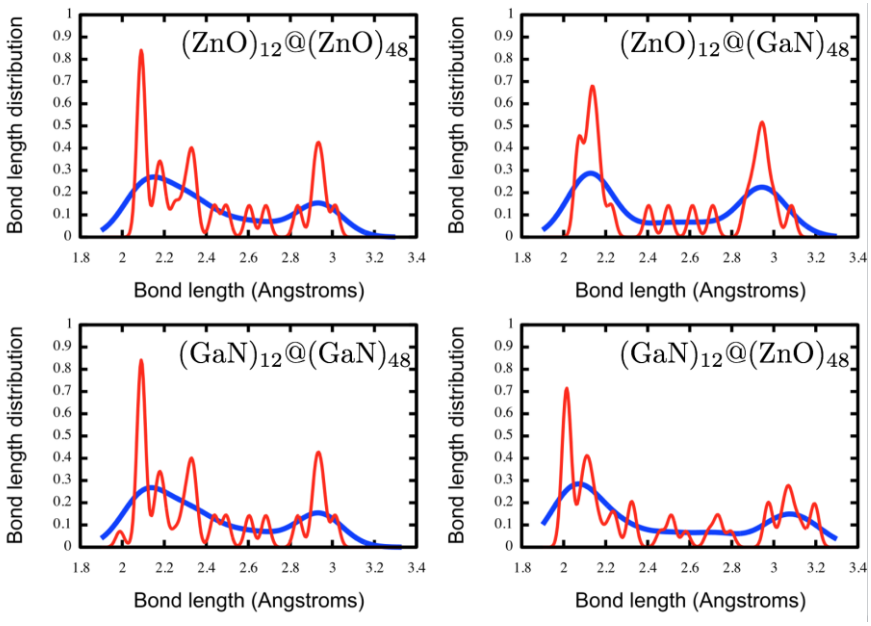

We observe that the pure double-bubble clusters have similar bond distributions, and notice only a difference of a small peak at 2 Å for the pure GaN system, which appears as a shoulder on the 2.3 Å peak in the pure ZnO system. We mark this shoulder (at approximately 2.25 Å) as the split of the distribution into bonded and non-bonded linkages. The number of bonded linkages, in fact, is constant for all the systems except for $(ZnO)_{12}@(GaN)_{48}$ and has a value of twenty-four, which is related to the ideal T symmetry octahedral shape. In this type of linking, two extremes can be possible: four of the eight hexagonal rings form drums with the outer bubble, or only half of the possible bonds are formed in such drums—see Figure 3b. The $(ZnO)_{12}@(GaN)_{48}$ double bubble, in contrast, has only twenty-two bonded linkages, which is not due to an inner bubble displacement from the centre of the outer bubble but is caused by a distortion in the outer bubble. To relate these observations to macroscopic properties of the systems, we considered the deformation as seen from the displacement of the centre of mass (COM) of the inner bubbles with respect to the outer bubbles, and their normalized second moments of atom distribution, as given in Table 2.

Table 2. Centre of mass (COM) differences and normalised second moments of atom distributions for the double bubble clusters (*x*, *y*, *z* coordinates).

System	COM difference (COM_{Outer}–COM_{Inner})	Normalised second moments of atom distribution	
		Inner	Outer
$(GaN)_{12}@(ZnO)_{48}$	0.00, 0.11, 0.05	1.05, 1.01, 0.94	1.05, 1.01, 0.94
$(ZnO)_{12}@(GaN)_{48}$	0.00, 0.00, 0.01	1.02, 1.00, 0.98	1.01, 1.00, 0.99
$(ZnO)_{12}@(ZnO)_{48}$	0.00, 0.00, 0.04	1.09, 1.00, 0.91	1.05, 1.00, 0.95
$(GaN)_{12}@(GaN)_{48}$	0.00, 0.01, −0.06	1.04, 1.01, 0.96	1.04, 1.01, 0.95

The largest COM displacement is seen in the $(GaN)_{12}@(ZnO)_{48}$ system and smallest in the inverse $(ZnO)_{12}@(GaN)_{48}$ system. The deformation is also lowest in the latter system, but has the largest values in pure ZnO. We explain this behaviour by considering the relative sizes of the inner and outer bubbles: the larger ZnO inner bubble fills in the space offered by the smaller GaN outer bubble better than the GaN counterpart. An additional point to take into account is the greater flexibility of the ZnO bubbles as compared with GaN: the size mismatch between the inner and outer bubble is accommodated easier by ZnO, the bubbles of which show the greater deformations. This flexibility is also seen in the bulk framework systems as discussed in Section 3.2 below. We show in Table 3 the energy of association, E_{Assoc}, calculated as the difference in total energy of the double bubble cluster from their moieties, *i.e.*, the $n_1 = 12$ and $n_2 = 48$ bubbles, and formation enthalpy, H_f,:

$$H_f = \frac{E_{DB} - [n_1(E_a) + n_2(E_b)]}{n_1 + n_2}, \quad (2)$$

where E_{DB} is the total energy of the double bubble cluster, E_a and E_b are the total energies of the pure bulk wurtzite structures, where *a* and *b* can be ZnO or GaN. We find that the formation of the double bubble systems is most favourable for the $(GaN)_{12}@(ZnO)_{48}$ system and least favourable for the inverse system, and that the pure double bubbles have equal formation energies.

Table 3. Energy of association, E_{Assoc} of single-shell cages and enthalpy of formation, H_f per atom for double bubble clusters as defined in Equation (2).

System	E_{Assoc} (kJ/mol)	H_f (kJ/mol)
$(GaN)_{12}@(ZnO)_{48}$	−11.27	78.32
$(ZnO)_{12}@(GaN)_{48}$	−8.17	104.55
$(ZnO)_{12}@(ZnO)_{48}$	−9.38	68.50
$(GaN)_{12}@(GaN)_{48}$	−9.16	116.18

We find that the formation of the homogeneous $(ZnO)_{12}@(ZnO)_{48}$ system is the most favourable closely followed by the heterogeneous $(GaN)_{12}@(ZnO)_{48}$ system compared to the homogeneous bulk wurtzite phases. Systems that have an outer-bubble of GaN are less likely to form when compared with bulk (at zero temperature). If we consider the mixing energies per atom:

$$E_{mix} = \frac{E_{DB} - [0.8(E_a) + 0.2(E_b)]}{120} \quad (3)$$

where E_a and E_b are the energies of the pure double bubbles that make up the mixed system, we find that the energy of mixing for $(GaN)_{12}@(ZnO)_{48}$ and $(ZnO)_{12}@(GaN)_{48}$ are 0.07 kJ/mol and −0.96 kJ/mol respectively.

3.2. Double Bubble Frameworks

We took the double bubble frameworks that were constructed using the procedure discussed in Section 2, and also corresponding systems of pure ZnO and GaN, and optimised their geometry (see Section 4.2 for details). The structural analysis performed in Section 3.1 was repeated for these frameworks. The calculated average bond lengths are presented in Table 4, again separated into inner-bubble bonds, outer-bubble bonds and, inter-layer bubble bonds (bonds connecting the inner to the outer bubbles). The graphs of the corresponding bond-length distribution analysis can be seen in Figure 6. Table 4 also has two additional pieces of information—the lattice parameter and the bulk modulus, which are available for these extended crystalline frameworks. Similar to the double bubble clusters, we find that the bonds in the ZnO inner bubble are slightly larger than the equivalent GaN bonds. In the framework systems this has a noticeable effect on the bond distribution: when the inner bubble is composed of ZnO, the bond length distribution is no longer bi-modal but has a single peak at 2.3 Å (Figure 6), which, similar to the double bubble clusters, is due to the larger ZnO bubble occupying the space inside the outer bubble. In this case, however, as the outer bubble is in a framework, it is unable to deform to the same degree as the gas-phase cluster, and only a single peak forms in the bond length distribution.

We also see that the lattice parameters for the double bubble frameworks are, as expected, related to the composition of the outer bubble, and that when the outer bubble is composed of ZnO the lattice parameters are larger. Comparing the bulk moduli of the systems, we find that the pure GaN system is the least compressible, whereas the pure ZnO system is the most. This agrees with the double bubble cluster findings, where the ZnO systems exhibit the greatest deformations. Table 5 shows the corresponding structural parameters for the wurtzite systems used in the framework analysis, and the bulk modulus of the GaN system is much larger than that of the ZnO.

Table 4. Structural parameters of double bubble frameworks. (Number in parentheses indicates standard error).

System	Lattice parameter (Å)	Bulk modulus (GPa)	D_{outer} (Å)	D_{inner} (Å)	D_{inter} (Å)	
					A	*B*
$(GaN)_{12}@(ZnO)_{48}$	19.26	78.84	1.96	1.94	2.08 (0.1)	2.96 (0.2)
$(ZnO)_{12}@(GaN)_{48}$	18.84	77.88	1.90	2.01	2.27 (0.1)	-
$(ZnO)_{12}@(ZnO)_{48}$	19.26	69.78	1.94	2.00	2.26 (0.0)	-
$(GaN)_{12}@(GaN)_{48}$	18.94	101.92	1.93	1.94	2.18 (0.2)	3.04 (0.1)

Figure 6. Bond distribution plots for the double bubble frameworks. Red line: Dispersion of Gaussian = 0.02, Blue line: Dispersion of Gaussian = 0.1.

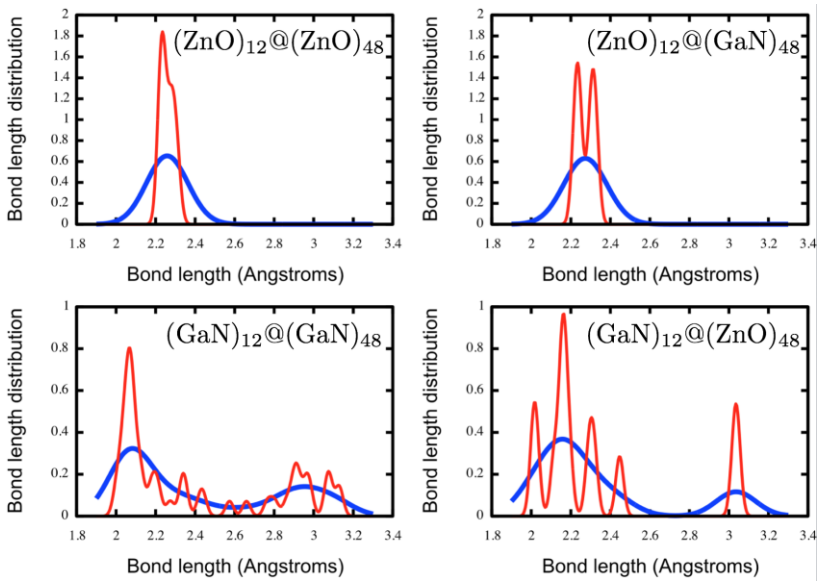

Table 5. Structural parameters of wurtzite phases.

System	Lattice parameter, *a* (Å)	Lattice parameter, *c* (Å)	Bulk modulus (GPa)	*u*
ZnO	3.251	5.204	146.136	0.382
GaN	3.187	2.760	188.367	0.378

We observe that the framework system of $(GaN)_{12}@(ZnO)_{48}$ has a similar inter-bond length distribution to that found in the double bubble systems which is again due to the fact that the smaller GaN cage has more freedom to move inside the larger ZnO bubble. The $(GaN)_{12}@(ZnO)_{48}$ system has a more clearly defined bi-modal distribution for the framework systems than observed for the double bubble cluster systems, and is likely due to reduced degrees of structural freedom with the extended bulk framework. Table 6 gives the formation enthalpies for the framework systems, and although these energies are positive *i.e.*, unfavourable with respect to the pure bulk wurtzite phases, they are small enough to be accessible at experimental temperatures, and are comparable to the formation of fullerene (C_{60}) with respect to bulk carbon (*ca.* 40 kJ/mol) [25,26]. The pure GaN double bubble framework was found to be the least likely to form, whereas the $(GaN)_{12}@(ZnO)_{48}$ framework was found to be most favourable—again agreeing with the formation energy double bubble cluster findings.

Table 6. Enthalpy of formation per atom of double bubble frameworks as defined in Equation (2).

System	H_F/atom (kJ/mol)
$(GaN)_{12}@(ZnO)_{48}$	13.17
$(ZnO)_{12}@(GaN)_{48}$	21.46
$(ZnO)_{12}@(ZnO)_{48}$	18.54
$(GaN)_{12}@(GaN)_{48}$	27.71

When we compare the energies of mixing (using Equation (3)) we find that the energies per atom for $(GaN)_{12}@(ZnO)_{48}$ and $(ZnO)_{12}@(GaN)_{48}$ are 1.98 kJ/mol and −2.61 kJ/mol, respectively.

4. Computational Detail

4.1. Interatomic Potentials Calculations

We have used the semi-classical GULP code [27] to construct and optimise ZnO structures prior to refining them with DFT. We employed polarisable shell inter-atomic potentials parameterised for bulk ZnO [7,28] in the double bubble cluster and framework calculations. The resulting atomic structures were used not only for ZnO, but also GaN and mixed ZnO/GaN structures; note that the bond lengths in GaN are very similar those in ZnO (see Tables 1–3 in Section 3), and we only required approximate initial atomic coordinates for input into the DFT calculations, as outlined below.

4.2. Density Functional Theory Calculations

In all of the *ab initio* calculations, we have used the solids-corrected Perdew-Burke-Ernzerhof (PBEsol) GGA exchange-correlation functional [29,30], and all structural optimisations were deemed converged when the atomic forces were less than 0.01 eV/Å.

A natural choice for the calculations on the double bubble clusters, due to its computational efficiency, is the DFT code FHI-aims [31] as it uses numeric atom-centred basis sets. These calculations were performed with the species defaults for the "tight" basis sets for accuracy (energies converged to 1 meV/atom) and with scalar ZORA relativistic treatment [32]. We have used the plane-wave DFT code VASP [33–36] to determined the equilibrium structures of the double bubble based framework (extended crystal systems—see Section 2), and, for comparison, wurtzite bulk ZnO and GaN. Within VASP, we employed the projector augmented wave (PAW) method [37] to describe the interactions between the cores (Zn:[Ar], Ga:[Ar], O:[He] and N:[He]) and the valence electrons.

To determine the equilibrium bulk structures avoiding the problem of Pulay stress, we have optimised the atomic coordinates at a series of different volumes, and fitted the resulting energy *versus* volume data to the Murnaghan equation of state.

We have found that for the framework systems, an energy cut-off of 500 eV, and Monkhorst-Pack *k*-point meshes of 8 × 8 × 6 and 1 × 1 × 1 for, respectively, the pure bulk wurtzite systems, and the $(A)_{12}@(B)_{48}$ systems, where A and B stand for either ZnO or GaN, provide convergence in total energy up to 10^{-5} eV for the framework systems, which is comparable with our double bubble cluster calculations.

5. Conclusions

We have constructed double-bubble clusters and frameworks of ZnO and GaN from a bottom up approach from cage structures analogous to fullerenes formed from hexagonal building units [15,16,22]. The four systems we have considered, $(GaN)_{12}@(ZnO)_{48}$, $(ZnO)_{12}@(GaN)_{48}$, $(ZnO)_{12}@(ZnO)_{48}$ and $(GaN)_{12}@(GaN)_{48}$, were first geometry optimized using a semi-empirical potential within the GULP code and then refined using FHI-aims (for the double bubble clusters) or VASP (for the frameworks) at the DFT level of theory using the PBEsol exchange-correlation functional. We found that although the average bond lengths of both ZnO and GaN are similar, the average bond lengths for ZnO inner bubbles were larger than the GaN inner bubbles of both the double bubble cluster systems and the frameworks. This relative size difference, we believe, means that the larger ZnO inner bubble fills in the space offered by the smaller GaN outer bubble better than the GaN counterpart. In addition, we found that the greater flexibility of the ZnO bubbles from calculations of bulk moduli, as compared with that of GaN bubbles, means that the size mismatch between the inner bubble and outer bubble is more readily accommodated by ZnO. Furthermore, the structural analysis of the pure ZnO double bubbles also showed the greater deformations. The average M-X inter-bubble bonds were found to exhibit a bi-modal distribution for both clusters and frameworks, except for the pure ZnO and $(ZnO)_{12}@(GaN)_{48}$ framework systems. These single-peak distributions were due to the larger ZnO inner bubble that has less freedom to move than in the inverse systems. The association energies of the double bubble clusters show that the systems investigated here are favourable when compared to individual bubbles, although when compared to bulk wurtzite phases, the clusters are less favourable.

The standard formation enthalpies for the framework systems are lower than those of carbon fullerenes. Therefore, we suggest that these double bubble systems should be thermodynamically accessible and could provide valuable material properties in the future.

Acknowledgments

We thank kindly our former collaborators Said Hamad, Eleonora Spano, Stefan T. Bromley, Stephen A. Shevlin, Matthew B. Watkins, and Abdullah A. Al-Sunaidi, discussions with who have been inspiring and instrumental for us undertaking this research. We also thank EPSRC for providing the funding for Matthew Farrow and Scott Woodley on grant numbers EP/I03014X9 and EP/K038958; John Buckeridge and Alexey Sokol on grant number EP/IO1330X; and Andrew Logsdail on grant numbers EP/I030662/1 and EP/K038419/1. The authors also acknowledge the use of the UCL Legion High Performance Computing Facility (Legion@UCL) and associated support services; the IRIDIS cluster provided by the EPSRC funded Centre for Innovation (EP/K000144 and EP/K000136); this work made use of the facilities of HECToR and ARCHER, the UK's national high-performance computing service through membership of the UK's HPC Materials Chemistry Consortium, which is funded by EPSRC (EP/L000202).

Author Contributions

The structures were constructed by Scott M. Woodley. The interatomic potential calculations were performed by Scott M. Woodley and Alexey A. Sokol. The double bubble cluster calculations were

performed by Matthew R. Farrow. The double bubble framework calculations were performed by John Buckeridge. The literature was researched by Andrew J. Logsdail and David O. Scanlon. Expertise both in relevant materials science and methodology was provided by C. Richard A. Catlow and Scott M. Woodley. Vital contributions to simulations design, the data analysis and preparation of the manuscript were made by all of the authors.

Conflicts of Interest

The authors declare no conflict of interest.

References

1. Fujishima, A.; Honda, K. Electrochemical photolysis of water at a semiconductor electrode. *Nature* **1972**, *238*, 37–38.
2. Vispute, R.D.; Talyansky, V.; Choopun, S.; Sharma, R.P.; Venkatesan, T.; He, M.; Tang, X.; Halpern, J.B.; Spencer, M.G.; Li, Y.X.; *et al.* Heteroepitaxy of ZnO on GaN and its implications for fabrication of hybrid optoelectronic devices. *Appl. Phys. Lett.* **1998**, *73*, 348–350.
3. Nakamura, S.; Pearton, S.; Fasol, G. *The Blue Laser Diode: The Complete Story*; Springer-Verlag: Berlin, Germany, 2000.
4. Yu, Q.-X.; Xu, B.; Wu, Q.-H.; Liao, Y.; Wang, G.-Z.; Fang, R.-C.; Lee, H.-Y.; Lee, C.-T. Optical properties of ZnO/GaN heterostructure and its near-ultraviolet light-emitting diode. *Appl. Phys. Lett.* **2003**, *83*, 4713.
5. Zhu, H.; Shan, C.-X.; Yao, B.; Li, B.-H.; Zhang, J.-Y.; Zhang, Z.-Z.; Zhao, D.-X.; Shen, D.-Z.; Fan, X.-W.; Lu, Y.-M.; *et al.* Ultralow-threshold laser realized in zinc oxide. *Adv. Mater.* **2009**, *21*, 1613–1617.
6. Shevlin, S.A.; Guo, Z.X.; van Dam, H.J.J.; Sherwood, P.; Catlow, C.R.A.; Sokol, A.A.; Woodley, S.M. Structure, optical properties and defects in nitride (III–V) nanoscale cage clusters. *Phys. Chem. Chem. Phys.* **2008**, *10*, 1944–1959.
7. Catlow, C.R.A.; French, S.A.; Sokol, A.A.; Al-Sunaidi, A.A.; Woodley, S.M. Zinc oxide: A case study in contemporary computational solid state chemistry. *J. Comput. Chem.* **2008**, *29*, 2234–2249.
8. Catlow, C.R.A.; Bromley, S.T.; Hamad, S.; Mora-Fonz, M.; Sokol, A.A.; Woodley, S.M. Modelling nano-clusters and nucleation. *Phys. Chem. Chem. Phys.* **2010**, *12*, 786–811.
9. Watkins, M.B.; Shevlin, S.A.; Sokol, A.A.; Slater, B.; Catlow, C.R.A.; Woodley, S.M. Bubbles and microporous frameworks of silicon carbide. *Phys. Chem. Chem. Phys.* **2009**, *11*, 3186–3200.
10. Woodley, S.M.; Watkins, M.B.; Sokol, A.A.; Shevlin, S.A.; Catlow, C.R.A. Construction of nano- and microporous frameworks from octahedral bubble clusters. *Phys. Chem. Chem. Phys.* **2009**, *11*, 3176–3185.
11. Carrasco, J.; Illas, F.; Bromley, S.T. Ultralow-density nanocage-based metal-oxide polymorphs. *Phys. Rev. Lett.* **2007**, *99*, 235502.
12. Hamad, S.; Catlow, C.R.A.; Spanó, E.; Matxain, J.M.; Ugalde, J.M. Structure and properties of ZnS nanoclusters. *J. Phys. Chem. B* **2005**, *109*, 2703–2709.

13. Al-Sunaidi, A.A.; Sokol, A.A.; Catlow, C.R.A.; Woodley, S.M. Structures of zinc oxide nanoclusters: As found by revolutionary algorithm techniques. *J. Phys. Chem. C* **2008**, *112*, 18860–18875.
14. Behrman, E.C.; Foehrweiser, R.K.; Myers, J.R.; French, B.R.; Zandler, M.E. Possibility of stable spheroid molecules of ZnO. *Phys. Rev. A* **1994**, *49*, R1543–R1546.
15. Jensen, F.; Toftlund, H. Structure and stability of C24 and B12N12 isomers. *Chem. Phys. Lett.* **1993**, *201*, 89–96.
16. Golberg, D.; Bando, Y.; Stephan, O.; Kurashima, K. Octahedral boron nitride fullerenes formed by electron beam irradiation. *Appl. Phys. Lett.* **1998**, *73*, 2441–2443.
17. Woodley, S.M. *Applications of Evolutionary Computation in Chemistry*; Springer: Berlin, Germany, 2004; Volume 110.
18. Woodley, S.M. Prediction of crystal structures using evolutionary algorithms and related techniques. In *Applications of Evolutionary Computation in Chemistry*; Springer-Verlag: Berlin, Germany, 2004; Volume 110, pp. 95–132.
19. Foster, M.D.; Friedrichs, O.D.; Bell, R.G.; Paz, F.A.A.; Klinowski, J. Structural evaluation of systematically enumerated hypothetical uninodal zeolites. *Angew. Chem.* **2003**, *115*, 4026–4029.
20. Zwijnenburg, M.A.; Illas, F.; Bromley, S.T. Apparent scarcity of low-density polymorphs of inorganic solids. *Phys. Rev. Lett.* **2010**, *104*, 175503.
21. Enyashin, A.N.; Gemming, S.; Bar-Sadan, M.; Popovitz-Biro, R.; Hong, S.Y.; Prior, Y.; Tenne, R.; Seifert, G. Structure and stability of molybdenum sulfide fullerenes. *Angew. Chem. Int. Ed.* **2007**, *46*, 623–627.
22. Parilla, P.A.; Dillon, A.C.; Jones, K.M.; Riker, G.; Schulz, D.L.; Ginley, D.S.; Heben, M.J. The first true inorganic fullerenes? *Nature* **1999**, *397*, 114.
23. Kasuya, A.; Sivamohan, R.; Barnakov, Y.A.; Dmitruk, I.M.; Nirasawa, T.; Romanyuk, V.R.; Kumar, V.; Mamykin, S.V.; Tohji, K.; Jeyadevan, B.; *et al.* Ultra-stable nanoparticles of CdSe revealed from mass spectrometry. *Nat. Mater.* **2004**, *3*, 99–102.
24. Botti, S.; Marques, M.A.L. Identification of fullerene-like cdse nanoparticles from optical spectroscopy calculations. *Phys. Rev. B* **2007**, *75*, 035311.
25. Diogo, H.P.; da Piedade, M.E.M.; Dennis, T.J.S.; Hare, J.P.; Kroto, H.W.; Taylor, R.; Walton, D.R.M. Enthalpies of formation of buckminsterfullerene (C_{60}) and of the parent ions C_{60}^{+}, C_{60}^{2+}, C_{60}^{3+} and C_{60}^{-}. *J. Chem. Soc. Faraday Trans.* **1993**, *89*, 3541–3544.
26. Curl, R.F.; Haddon, R.C. On the formation of the fullerenes. *Philos. Trans.* **1993**, *343*, 19–32.
27. Gale, J.D.; Rohl, A.L. The general utility lattice program (gulp). *Mol. Simul.* **2003**, *29*, 291–341.
28. Whitmore, L.; Sokol, A.A.; Catlow, C.R.A. Surface structure of zinc oxide (1010), using an atomistic, semi-infinite treatment. *Surf. Sci.* **2002**, *498*, 135–146.
29. Perdew, J.P.; Burke, K.; Ernzerhof, M. Generalized gradient approximation made simple. *Phys. Rev. Lett.* **1996**, *77*, 3865–3868.
30. Perdew, J.P.; Ruzsinszky, A.; Csonka, G.I.; Vydrov, O.A.; Scuseria, G.E.; Constantin, L.A.; Zhou, X.; Burke, K. Restoring the density-gradient expansion for exchange in solids and surfaces. *Phys. Rev. Lett.* **2008**, *100*, 136406.

31. Blum, V.; Gehrke, R.; Hanke, F.; Havu, P.; Havu, V.; Ren, X.; Reuter, K.; Scheffler, M. *Ab initio* molecular simulations with numeric atom-centered orbitals. *Comput. Phys. Commun.* **2009**, *180*, 2175–2196.
32. Van Lenthe, E.; Baerends, E.J.; Snijders, J.G. Relativistic total energy using regular approximations. *J. Chem. Phys.* **1994**, *101*, 9783.
33. Kresse, G.; Hafner, J. *Ab initio* molecular dynamics for liquid metals. *Phys. Rev. B* **1993**, *47*, 558–561.
34. Kresse, G.; Hafner, J. *Ab initio* molecular-dynamics simulation of the liquid-metal–amorphous-semiconductor transition in germanium. *Phys. Rev. B* **1994**, *49*, 14251–14269.
35. Kresse, G.; Furthmüller, J. Efficiency of *ab-initio* total energy calculations for metals and semiconductors using a plane-wave basis set. *Comput. Mater. Sci.* **1996**, *6*, 15–50.
36. Kresse, G.; Furthmüller, J. Efficient iterative schemes for *ab initio* total-energy calculations using a plane-wave basis set. *Phys. Rev. B* **1996**, *54*, 11169–11186.
37. Blöchl, P.E. Projector augmented-wave method. *Phys. Rev. B* **1994**, *50*, 17953–17979.